Available online at www.sciencedirect.com

ScienceDirect

Procedia Technology 15 (2014) 285 – 294

Procedia Technology

2nd International Conference on System-Integrated Intelligence: Challenges for Product and Production Engineering

Development of an intelligent cruise control using optimal control methods

Michael Dellnitz[a,b], Julian Eckstein[c], Kathrin Flaßkamp[b], Patrick Friedel[c], Christian Horenkamp[a,b], Ulrich Köhler[c], Sina Ober-Blöbaum[a,b], Sebastian Peitz[a,b]*, Sebastian Tiemeyer[c]

[a]*University of Paderborn, Institute for Industrial Mathematics, Warburger Str. 100, 33098 Paderborn, Germany*
[b]*University of Paderborn, Chair of Applied Mathematics, Warburger Str. 100, 33098 Paderborn, Germany*
[c]*HELLA KGaA Hueck & Co., Beckumer Str. 130, 59552 Lippstadt, Germany*

Abstract

In this contribution, the range extension problem of electric vehicles is addressed. To this aim, an intelligent cruise control is developed based on the formulation of an optimal control problem. Solutions of this optimal control problem are energy efficient accelerator pedal position profiles. They can be computed numerically by a direct optimal control method using sequential quadratic programming. The approach is applied to two different driving scenarios. The results show that the energy efficiency is increased by using optimal control for both an artificial and a realistic scenario.

Peer-review under responsibility of the Organizing Committee of SysInt 2014.

Keywords: Optimal Control; optimization; electric vehicles

1. Introduction

Alternative drive technologies have gained more and more attention during the last years. This is mainly due to an increasing awareness of the impact of CO_2 emissions on climate change and the limitation of fossil fuels. Thus, research focuses, for instance, on electrically powered vehicles. Up to now, electric vehicles (EV) suffer from a

* Corresponding author. Tel.: +49-5251-605022; Fax: +49-5251-605020;
E-mail address: speitz@ifim.upb.de

Peer-review under responsibility of the Organizing Committee of SysInt 2014.
doi:10.1016/j.protcy.2014.09.082

severely reduced range compared to conventional internal combustion engine powered vehicles. Firstly, this is caused by the high battery cost and, secondly, by the limited lithium ion battery storage density. Therefore, strategies to increase the EV range without enlarging the battery play an important role for electromobility (cf. e.g. [1], [2]).

In this contribution, an „intelligent cruise control“ is designed to optimize the drivetrain power uptake by taking into account topographic information of a prescribed travel route. Standard cruise controls, which have been originally developed for fossil-fueled vehicles, have been adapted in a number of recent publications. In [3] and [4], for instance, *model predictive control* is used for reducing the fuel consumption of heavy diesel trucks on a known topography. It is shown that the variation of the vehicle's velocity – within certain limits – has the potential to decrease the overall energy consumption. Applying this method to EVs allows for larger travel distances and thereby overcomes range anxiety or increases the energy available for comfort functions such as air conditioning.

The task of minimizing the energy consumption on a given route can be formulated as an *optimal control problem* with the aim to determine the accelerator pedal position profile with respect to minimum battery depth of discharge (DOD). Different methods exist to solve such optimal control problems: *Indirect methods* make use of the necessary optimality conditions from the Pontryagin Maximum Principle while *direct methods* are based on a discretization by which the problem is transformed into a nonlinear constrained optimization problem (cf. Section 3 for details). An overview of appropriate control strategies in the case of hybrid electric vehicles can be found in [5]. Constraints on thermal conditions are additionally taken into account in [6].

Various strategies have also been considered for EVs. In [7], the solution of the optimal control problem is computed by *dynamic programming* techniques. This method allows the computation of control sequences for arbitrary starting points. However, due to the nature of this method, it is restricted to low-dimensional problems. For the solution of a higher dimensional problem, an indirect method exploiting the special geometric structure of the EV model is used in [8].

In contrast to that, we evaluate the use of a direct optimal control method in combination with black-box simulations for this application. In order to apply this method to the EV optimal control problem, we neglect the virtual driver (cf. Section 2) and directly compute an optimal solution for the accelerator pedal position profile by discretizing it with respect to time. In combination with the vehicle dynamics simulation model the optimal control problem is transformed into a nonlinear restricted optimization problem. This time discretized accelerator pedal position profile leads to a large number of optimization parameters. This optimization problem is solved using a standard sequential quadratic programming (SQP) method (cf. e.g. [9]). We then compute several solutions for different slope profiles and investigate the influence of different discretizations and initial guesses on the quality of the solution.

The remainder of this article is organized as follows: In Section 2, the simulation model of an EV is described. The direct numerical method which is used for the solution of the corresponding optimal control problem is described in Section 3. In Section 4, the specific optimal control problem based on the simulation model is formulated and solved by the direct method introduced before. Finally, a conclusion can be found in Section 5.

2. Electric vehicle dynamics

2.1. Electric vehicle model

The central components of the chosen EV are the drivetrain (DT) and the high voltage (HV) battery (see Figure 1). In this article, HV refers to the traction circuit voltage level and low voltage (LV) refers to the 12 V circuit voltage level. The DT consists of two identical electric motors with an inverter attached to each of them. The simulation model is realized in MATLAB/Simulink. Basically, the model consists of an ideal PI controller which acts as a virtual driver, an electronic control unit (ECU) which holds the energy management and the pedal map, and the vehicle model (VM). The driver model requires a time dependent velocity profile $v(t)$ such as the New European Driving Cycle (NEDC) as input r_v (see Figure 2). The actuating variable is the accelerator pedal position u_{pp} which is transformed into a torque request y_τ by the ECU. To prevent a possible windup of the PI controller, conditional integration (*clamping*) has been used.

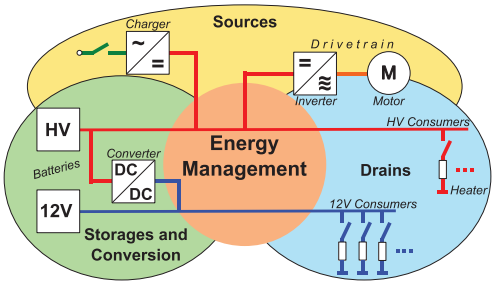

Fig. 1. Overview of electric vehicle components [10].

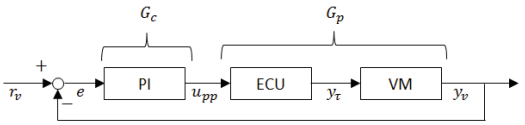

Fig. 2. Closed control loop with ideal PI controller.

The error e (cf. Figure 2), which is the difference between the actual velocity y_v and the desired velocity r_v, serves as an input for the ideal PI controller. It has been designed with a proportional gain of 80 and an integral gain of 0.05. This closed loop control system is validated in Section 2.2. However, the optimal control problem will be formulated for the open loop system with u_{pp} as the control variable (cf. Section 4). The VM consists of the submodels electrical system (ES), DT and vehicle resistance forces (VRF). The ES covers the HV and LV consumers, the LV battery, the DC/DC converter and the HV battery (see Figure 1). A detailed description of the ES can be found elsewhere [10]. The DT is represented by a backward simulation model. The link between the mechanical system and the electrical system is realized via a look-up table (LUT) which holds the motor efficiency map η_{mot} as a function of torque τ_m and speed ω_m. The electric motor power $P_{m,el}$ is related to the mechanical motor power $P_{m,mech}$ by

$$P_{m,el} = P_{m,mech} \cdot [\eta_{mot}(\omega_m, \tau_m)]^{-1} = \tau_m \cdot \omega_m \cdot [\eta_{mot}(\omega_m, \tau_m)]^{-1}. \quad (1)$$

Similar to the motors, the inverters are realized by a LUT incorporating the efficiency η_{inv} as a function of the effective output (phase) current I_m. The inverter power P_{inv} is linked to $P_{m,el}$ by (2). I_m is calculated using $P_{m,el}$, the HV battery voltage V_{HV}, the constant power factor $cos\varphi$ and the so-called (variable) modification factor f_{mod}. The additional factor $\sqrt{3/2}$ serves as conversion factor from DC to AC.

$$P_{inv} = P_{m,el} \cdot [\eta_{inv}(I_m)]^{-1}, \qquad I_m = P_{m,el} \cdot \left(f_{mod} \cdot V_{HV} \cdot cos\varphi \cdot \sqrt{3/2}\right)^{-1} \quad (2)$$

The VRF submodel contains the vehicle longitudinal dynamics as explained in detail in [10]. Here, ODEs describe the motion influenced by air drag, rolling resistance, grade resistance, and propulsion.

2.2. Model validation

In order to validate the simulation model, several test drives have been recorded and compared to the corresponding simulation results. The general procedure was to log the HV battery state of charge (SOC), the velocity, the motor torque, the motor current, the DC/DC current, and the ambient temperature. Furthermore, a GPS tracker was used to record topography data. The test drives have either been performed on a temperature-controlled dynamometer or on public roads with moderate weather conditions and very low wind speeds. On the dynamometer the NEDC has been used. Input data to the simulation were the SOC at the beginning, the mean DC/DC current to eliminate the influence of LV consumers, the mean environmental temperature and, if present, the altitude as well as the actual velocity of the EV.

In this article, we focus on the model validation with regard to the HV battery SOC, since it expresses the quality of the simulation concerning the consumption most significantly. When comparing the measured and the simulated test drive, the mean deviation $\boldsymbol{D_{mean,SOC}}$ as well as the absolute mean deviation $\boldsymbol{D_{abs,SOC}}$ have been chosen as relevant quantities. Both evaluation parameters are relative values with regard to the test drive:

$$D_{mean,SOC} = \frac{\int_0^T \Delta SOC(t)\, dt}{\int_0^T SOC_{meas}(t) - \min_{\kappa}(SOC_{meas}(\kappa))\, dt},\ D_{abs,SOC} = \frac{\int_0^T |\Delta SOC(t)| dt}{\int_0^T SOC_{meas}(t) - \min_{\kappa}(SOC_{meas}(\kappa))\, dt}, \tag{3}$$

with $\boldsymbol{\Delta SOC(t) = SOC_{meas}(t) - SOC_{sim}(t)}$ denoting the difference of the state of charge between measurement and simulation.

Further evaluation parameters are the relative difference $\boldsymbol{D_{end,SOC}}$ at the end of the test drive and the maximum deviation $\boldsymbol{D_{max,SOC}}$ over the entire test drive:

$$\boldsymbol{D_{end,SOC} = \frac{\Delta SOC(T)}{\max_{\kappa}(SOC_{meas}(\kappa)) - \min_{\kappa}(SOC_{meas}(\kappa))},\ D_{max,SOC} = \max_{\kappa}(|\Delta SOC(\kappa)|).} \tag{4}$$

The results of the validation for two test tracks with different topographies are given in Table 1. It can be observed that for track A there is a remarkable match of test drive measurements and simulations: $\boldsymbol{D_{mean}}$ is below 1 % and both $\boldsymbol{D_{abs,SOC}}$ and $\boldsymbol{D_{max,SOC}}$ are below 2 %. When additionally considering the topography data in the simulation, the accuracy is significantly improved (cf. Table 1, col. 1 versus col. 2 and col. 3 vs. col. 4): For track B (see Figure 3), $\boldsymbol{D_{max,SOC}}$ is reduced by a factor of more than 4 from 17.54 % to 3.76 %. The corresponding SOC profiles are visualized in Figure 4. Even for the rather flat track A an improvement can be seen with the topography data for $\boldsymbol{D_{max,SOC}}$, $\boldsymbol{D_{abs,SOC}}$, and $\boldsymbol{D_{end,SOC}}$. A reason for flat tracks having a lower deviation than hilly tracks (by more than a factor of 2) may lie in the inaccuracy of the topography data.

Table 1: Evaluation parameters showing the deviation of the SOC for four pairs of simulation and test drive comparisons in %. Track A represents a rather flat road, while track B represents a rather hilly road with altitude differences of more than 75 m. The computations in which the topography data has been used in the simulation are marked with (topo).

	Test drive on track A	Test drive on track A (topo)	Test drive on track B	Test drive on track B (topo)
$D_{mean,SOC}$	0.41	0.52	-16.56	2.25
$D_{abs,SOC}$	1.71	1.00	16.57	2.58
$D_{end,SOC}$	1.63	1.30	-8.00	3.47
$D_{max,SOC}$	1.93	1.40	17.54	3.76

In conclusion, the simulation is in very good agreement with the measured values for the HV battery SOC. Furthermore, the implementation of topography data enables the simulation to adequately model drives on tracks with variable altitude. However, the results depend on the resolution of the topography data.

In general, there is also a very good agreement between simulations and measurements concerning the vehicle velocity (results not shown due to space limitations). The mean and the absolute deviation of the velocity profile are strictly below 0.1 % and 3 %, respectively. Thus, it can be concluded as well that the driver model follows the given velocity profile adequately. This is another necessary condition for evaluating the simulation quality. Altogether, as the validation of the Simulink model shows, the model is adequate to be used for consumption optimization.

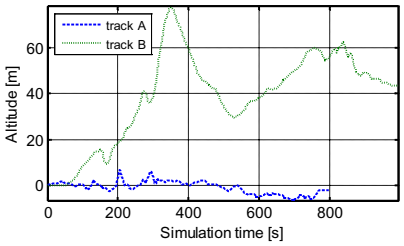

Fig. 3. Altitude profile of tracks as function of time.

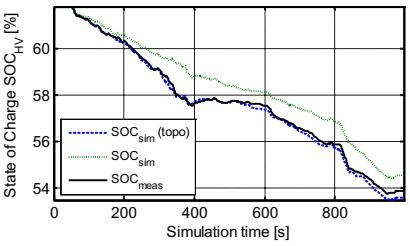

Fig. 4. HV battery SOC of track B as function of time.

3. Optimal control

In this section, we introduce a formal mathematical problem setting and present state of the art numerical solution techniques for optimal control problems. Subsequently, these are applied to the range extension problem of an EV in Section 4.

3.1. Problem formulation

Optimal control aims at finding a control profile which solves the control problem, e.g. steering the system from an initial point to a desired final point in a given time, and which, at the same time, minimizes a given cost functional J. Formally, an optimal control problem is stated as

$$\min_{\boldsymbol{u}} J(\boldsymbol{x},\, \boldsymbol{u}) = \int_0^T C(\boldsymbol{x}(t),\, \boldsymbol{u}(t))dt + \psi\big(\boldsymbol{x}(T)\big) \tag{5}$$

with respect to

$$\dot{\boldsymbol{x}}(t) = \boldsymbol{f}\big(\boldsymbol{x}(t),\, \boldsymbol{u}(t)\big)\ \forall\, t \in [0,T], \tag{6}$$

$$\boldsymbol{g}\big(\boldsymbol{x}(0),\, \boldsymbol{x}(T)\big) = \boldsymbol{0}, \tag{7}$$

$$\boldsymbol{h}\big(\boldsymbol{x}(t),\, \boldsymbol{u}(t)\big) \geq \boldsymbol{0}\ \forall\, t \in [0,T], \tag{8}$$

$$\boldsymbol{b_l} \leq \begin{pmatrix}\boldsymbol{x}(t)\\ \boldsymbol{u}(t)\end{pmatrix} \leq \boldsymbol{b_u}\ \forall\, t \in [0,T]. \tag{9}$$

As usual, the cost functional $\boldsymbol{J}$ is given in integral formulation with an additional final cost function $\boldsymbol{\psi}$ (cf. (5)) and depends on the system's state trajectory $\boldsymbol{x}$ as well as on the control $\boldsymbol{u}$. For a given control profile $\boldsymbol{u}$, the state trajectory can be obtained from the system's controlled dynamics, which are determined by the ordinary differential equation (6). Further constraints that have to be taken into account are the boundary conditions $\boldsymbol{g}$ (cf. (7)), e.g. fixed initial and final states, the path constraints $\boldsymbol{h}$ (cf. (8)), i.e. technical constraints on states or controls given pointwise in time, or box constraints (cf. (9)) defined by maximal/minimal states and controls $\boldsymbol{b_l}$ and $\boldsymbol{b_u}$, respectively.

Optimal control problems for complex, nonlinear dynamical systems have to be solved by appropriate numerical techniques. As discussed in Section 1, state of the art approaches can be divided into two classes, cf. [11] for an overview. Direct methods have proven to be well suitable for real world applications in the last years. We will describe this approach in more detail in the following and present the application to the EV-related optimal control problem subsequently.

3.2. Direct numerical methods

A discretization of an optimal control problem starts with a discretization of the control profile. Therefore, a time grid $\Delta t = \{t_0 = 0, t_1, \dots, t_{N-1}, t_N = T\}$ is defined which leads to a discrete control trajectory $\boldsymbol{u_d} = \{\boldsymbol{u_k}\}_{k=0}^{N-1}$ with $\boldsymbol{u_k}$ being an approximation of $\boldsymbol{u}(t_k)$. Then, the $N+1$ controls $\boldsymbol{u_k},\ k = 0, \dots, N$, form the optimization parameters of the nonlinear optimization problem (cf. (10)-(12)). The corresponding discrete state trajectory $\boldsymbol{x_d} = \{\boldsymbol{x_k}\}_{k=0}^{N}$ is obtained from a numerical integration scheme $\boldsymbol{\Phi_h}$ applied to the differential equation (11), where $\boldsymbol{x_k}$ is an

approximation of $\boldsymbol{x}(t_k)$. The quality of the approximation of the real continuous time solution depends on the order of the chosen integrator (cf. e.g. [12]). The integral of the cost functional (cf. (5)) can be approximated by quadrature rules on Δt leading to the discrete cost function J_d in (10). Together with a discretization of the path and box constraints (cf. (12)), we obtain the following nonlinear restricted optimization problem

$$\min_{\boldsymbol{u_d}} J_d(\boldsymbol{x_d}, \boldsymbol{u_d}) = \sum_{k=0}^{N-1} C_d(\boldsymbol{x_k}, \boldsymbol{u_k}) + \psi_d(\boldsymbol{x_N}) \tag{10}$$

with respect to

$$\boldsymbol{x_{k+1}} = \boldsymbol{\Phi_h}(\boldsymbol{x_k}, \boldsymbol{u_k}), \tag{11}$$

$$\boldsymbol{g_d}(\boldsymbol{x_0}, \boldsymbol{x_N}) = \boldsymbol{0}, \boldsymbol{h_d}(\boldsymbol{x_d}, \boldsymbol{u_d}) \geq \boldsymbol{0}, \boldsymbol{b_l} \leq \begin{pmatrix} \boldsymbol{x_d} \\ \boldsymbol{u_d} \end{pmatrix} \leq \boldsymbol{b_u}. \tag{12}$$

Sequential quadratic programming (SQP, cf. e.g. [9]) is an efficient method for solving high dimensional nonlinear optimization problems and is nowadays implemented in many software tools. The basic idea is to sequentially formulate auxiliary quadratic problems in order to approximate a (locally) optimal solution of the original problem. As for most nonlinear optimization methods, the solution obtained by SQP strongly depends on initial guesses. The SQP method requires derivatives of the cost function and the constraints. Since these cannot be computed analytically for large nonlinear dynamical systems, the derivatives either have to be computed by automatic differentiation or they can be numerically approximated by finite differences.

4. Intelligent cruise control

When allowing the vehicle velocity to vary, the formalism described in Section 3 can now be applied to the EV model in order to reduce its battery discharge (cf. Section 4.1). Therefore, the closed loop system is replaced by a system with the accelerator pedal position profile as an (open loop) control input. Neglecting recuperation (which only occurs when the pedal position is exactly zero), the dynamical behavior of the EV can be assumed to be sufficiently smooth so that the SQP method is applicable. In Section 4.2, an artificial track of four increasingly steep plateaus is used to identify the optimal control method's potential as well as to show the local nature of the solution. In Section 4.3, the method is applied to the measured track that has been used for the validation in Section 2.2 to show that it also yields a reduced energy consumption in a realistic scenario. Solutions for discretizations between one and 200 variables have been calculated. Due to space limitations, only a few representative results are shown.

4.1. Problem formulation

In the optimal control problem ((5) - (9)), one can set the control $\boldsymbol{u_{pp}}$ to the accelerator pedal position and the cost functional in (5) only consists of a final cost, i.e. $\boldsymbol{J} = -\boldsymbol{SOC}(\boldsymbol{T})$, the negative state of charge at final time $\boldsymbol{T}$ (cf. (13)). Note that the SOC implicitly depends on the control $\boldsymbol{u_{pp}}$ as well as on the system's internal states. The system dynamics (6) are represented by the Simulink model of the EV with states $\boldsymbol{x} = (\boldsymbol{s}, \boldsymbol{v})$, where $\boldsymbol{s}$ and $\boldsymbol{v}$ denote position and velocity, respectively. The differential equation is solved by the Simulink solver *ode3*. The velocity at the boundaries $\boldsymbol{t} = \boldsymbol{0}$ **and** $\boldsymbol{t} = \boldsymbol{T}$ is set to the average value of 25 m/s (cf. (15)). Similar to a standard cruise control, a certain minimal average velocity ($\overline{\boldsymbol{v_{min}}} = \boldsymbol{s_{min}}/\boldsymbol{T}$) is desirable. Consequently, for a fixed time interval $[\boldsymbol{0}, \boldsymbol{T}]$, the EV has to travel a minimal distance $\boldsymbol{s_{min}}$, which leads to the constraint (16). Finally, the accelerator pedal position is limited at every time $\boldsymbol{t}$ which is accounted for by the box constraint (17). Altogether, the following optimal control problem can be formulated:

$$\min_{u_{pp}}(-SOC(T)) \tag{13}$$

with respect to

$$\dot{\boldsymbol{x}}(t) = \boldsymbol{f}\left(\boldsymbol{x}(t), u_{pp}(t)\right) \; \forall \, t \in [0, T], \qquad \text{(Simulink model)} \tag{14}$$

$$v(0) = v(T) = 25 \text{ m/s}, \tag{15}$$

$$\int_0^T v(t)dt \geq s_{min}, \tag{16}$$

$$0 \leq u_{pp}(t) \leq 100 \; \forall \, t \in [0, T]. \tag{17}$$

The first step of the direct solution method is to define a time grid for the discrete control trajectory. In between the time nodes, the control is approximated by piecewise cubic Hermite interpolation, such that the differential

equations can be solved on a refined time grid. Then, since the dynamics is given by a Simulink model, the discretization is automatically performed by simulating the model with the approximated control trajectory $u_{pp,d}$ as the input and with the state of charge at time T as well as the approximated state trajectory $\boldsymbol{x_d}$ as output. Finally, the SQP method of the Matlab function *"fmincon"* is applied to the discretized problem. In the simulation, the first and second derivatives of the cost function and the boundary conditions with respect to states $\boldsymbol{x}$ and control u_{pp} have been approximated numerically using finite differences. This may prove problematic when using a model with nonsmooth subfunctions, e.g. caused by look-up tables. Therefore, optimality cannot be guaranteed in a strict mathematical sense. Nevertheless, as the results show, a considerable DOD reduction is observed.

4.2. Numerical results for an artificial track

An artificial track consisting of four plateaus with consecutively steeper but constant slopes was developed (see bottom plots of Figure 5 (a) – (d)). The minimal average velocity within the defined time interval $[0, T]$ with $T = 600$ s was set to $\overline{v_{min}} = 25\ \mathrm{m/s}$. In Figure 5, four different solutions of this optimal control problem differing in discretization and initial guess are shown. The corresponding numerical results are compared in Table 2. In the simplest case, the optimization is performed with only one variable leading to a constant accelerator pedal position profile (see Figure 5 (a)). Here, the initial pedal position is reduced as much as the constraints allow for such that only the minimal distance ($s_{min} = 15$ km) is reached. Using this result as an initial guess for a profile discretization with 200 points leads to a reduction of the battery DOD of approximately 3.5 %. It is interesting to see that – as one might expect – an increased accelerator pedal position on positive slopes is beneficial for the EV efficiency. As a result, the variation in velocity is reduced. Based on the observation that this reduction of velocity variance seems favorable for the efficiency, another objective function was formulated, namely the minimization of the velocity variance in the discretization points:

$$\min_{u_{pp}} \int_0^T (v(t) - \bar{v})^2 dt \approx \min_{u_{pp,d}} \sum_{k=0}^{N-1} \frac{h}{2} ((v_k - \bar{v})^2 + (v_{k+1} - \bar{v})^2), \tag{18}$$

where $\bar{v} = \frac{1}{N+1} \sum_{k=0}^{N} v_k$ is the average velocity and h is the constant time step. Following this approach, a DOD reduction of 5.4 % is achieved (cf. Figure 5 (c) and Table 2). Due to the local nature of the SQP method, a second SOC optimization has been performed using the result from (18) as initial guess. Although the discretization is much coarser in this case, this profile leads to the highest DOD reduction of approximately 5.6 %.

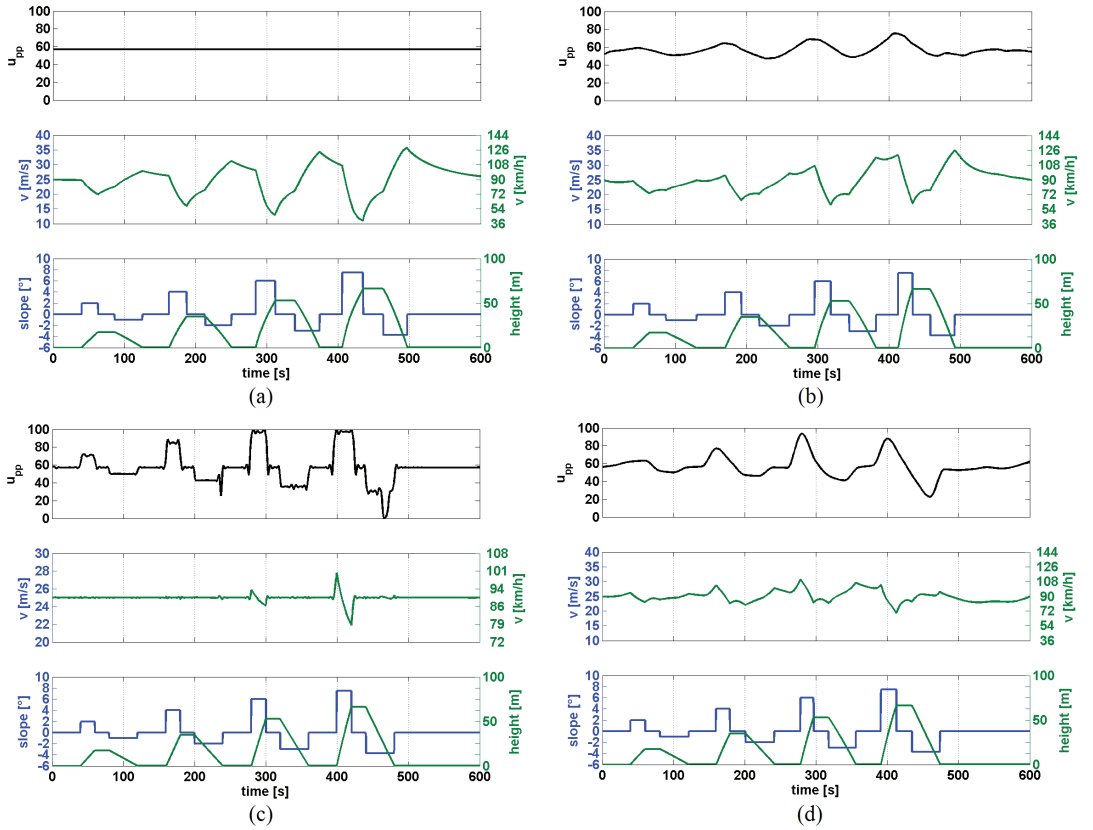

Fig. 5. Accelerator pedal position u_{pp} (top), EV velocity (middle) and track inclination/height (bottom) over time on an artificial track for different cost functionals, discretizations and initial guesses; (a) $J = -SOC(T)$, $u_{pp} = const.$, initial guess: $u_{pp} = 70 = const.$; (b) $J = -SOC(T)$, $N = 200$, initial guess: (a); (c) $J = \sum(v_i - \bar{v})^2$, $N = 200$, initial guess: (a); (d) $J = -SOC(T)$, $N = 30$, initial guess: (c).

Table 2. Comparison of the different solutions of the optimal control problem; the case descriptions (a) to (d) refer to the plots in Figure 5.

	(a)	(b)	(c)	(d)
Cost functional	$\min(-SOC(T))$	$\min(-SOC(T))$	$\min \sum(v_i - \bar{v})^2$	$\min(-SOC(T))$
Discretization	$u_{pp} = const.$	$N = 200$	$N = 200$	$N = 30$
Initial guess	Const. value $u = 70$	Solution of (a)	Solution of (a)	Solution of (c)
SOC(T)	0.9097	0.9129	0.9146	0.9148
DOD(T)	0.0903	0.0871	0.0854	0.0852
ΔDOD to (a)		-3.5 %	-5.4 %	-5.6 %

4.3. Numerical results for a real test track

Having demonstrated the capability of the method for an artificial track, the next step is to show that a DOD reduction can also be achieved for a realistic case. For this reason, the optimal control method presented above is applied to the track which has been measured during the model validation (cf. Section 2.2). The boundary conditions are chosen in order to match the test drive:

$$s_{min} = 28.752\ \text{km};\ T = 1000\ \text{s} \Rightarrow \overline{v_{min}} = 28.752\ \frac{\text{m}}{\text{s}} = 103.5\ \frac{\text{km}}{\text{h}},$$
$$v(0) = v(T) = 25\ \frac{\text{m}}{\text{s}}. \tag{19}$$

In Figure 6, the results of the optimization with two different initial guesses are shown, a comparison of the numerical results can be found in Table 3. As a result of the local nature of the SQP method, an initial guess $u_{pp} = const.$ (Figure 6 (a)) leads to an entirely different solution than an initial guess which results from the minimization of the velocity variance (Figure 6 (b)). In both cases, the differences between the initial guess and the optimized solution are fairly low in regions with low inclinations whereas stronger deviations occur at times where notable changes in the slope exist (e.g. at $t \approx 800\ s$).

Table 3: Comparison of the different solutions of the optimal control problem to the measurements; the scenarios (a) and (b) refer to the plots in Figure 6 where scenarios 1 and 2 are the initial guess and the optimized solution, respectively

	Measured	Scenario (a 1)	Scenario (a 2)	Scenario (b 1)	Scenario (b 2)
Cost functional	-	$\min(-SOC(T))$	$\min(-SOC(T))$	$\min \sum (v_i - \bar{v})^2$	$\min(-SOC(T))$
Discretization	-	$u_{pp} = const.$	200 points	100 points	100 points
SOC(T)	0.7538	0.7877	0.7923	0.7912	0.7935
DOD(T)	0.2462	0.2123	0.2077	0.2088	0.2065
ΔDOD to Measured	-	-13.6 %	-15.64 %	-15.19 %	-16.1 %
ΔDOD to Sc. (a 1)	-	-	-2.17 %	-1.65 %	-2.7 %

Similar to Section 4.2, the best result in terms of DOD reduction is achieved by minimizing the cost function (13) with a velocity variance minimizer (cf. (18)) as the initial guess (Scenario (b 2) in Table 3). In contrast to the results concerning the artificial track, using velocity variance minimization only (Scenario (b 1)) does not yield a result superior to the DOD minimization with a constant initial guess (Scenario (a 2)). The maximally achieved reduction of 2.7 % is less than for the artificial track, which is not surprising because the test track has mild slopes in most parts and parts with strong changes in the slope appear to offer the highest potential for the optimization method presented in Section 4.1.

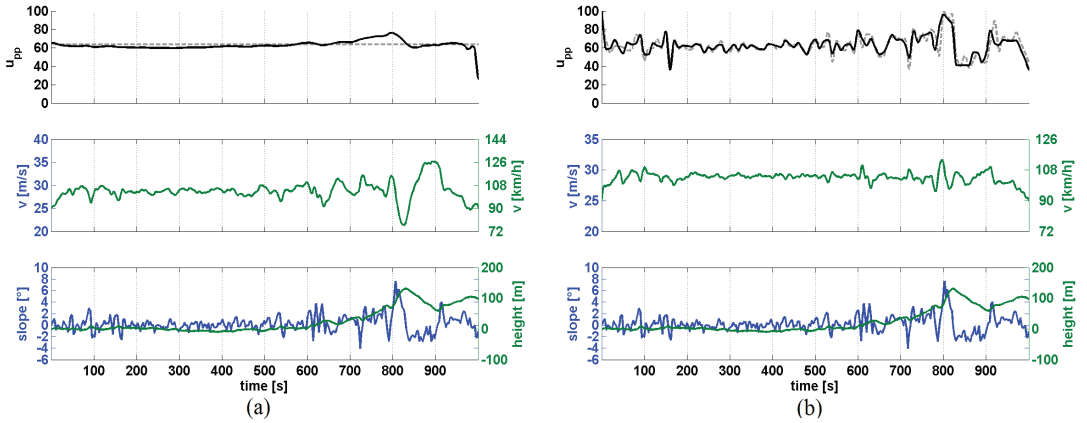

Fig. 6. Accelerator pedal position u_{pp} (top), EV velocity (middle) and track inclination/height (bottom) over time on a measured track for different discretizations and initial guesses; (a) $J = -SOC(T)$; $N = 200$; initial guess: $u_{pp} = 65 = const.$ (dashed line); (b) $J = -SOC(T)$; $N = 100$; initial guess: $\min \sum (v_i - \bar{v})^2$ with $N = 100$ (dashed line).

5. Conclusions

In this contribution, optimal control problems have been formulated and solved in order to minimize the depth of discharge of an electric vehicle on prescribed tracks. The direct optimal control solution method has proven to be well applicable since it has been possible to reduce the depth of discharge for the artificial as well as for the realistic scenario compared to a constant accelerator pedal position. However, one observes a strong dependence of the solutions on the initial guesses. Therefore, combined strategies with varying discretization points and even varying objectives have been tested, and this way, the highest depth of discharge reduction could be obtained. In future work, global optimization techniques will be used and the control problem can be studied with respect to several different objectives: Besides the energy efficiency, also the deviation from the mean velocity or the driven distance can serve as additional, probably conflicting objectives. These multiobjective optimization problems will be solved using the software package GAIO (cf. [13]).

Acknowledgements

This research was partially funded by the German Federal Ministry of Education and Research (BMBF) within the Leading-Edge Cluster “Intelligent Technical Systems OstWestfalenLippe” (it’s OWL) and managed by the Project Management Agency Karlsruhe (PTKA).

References

[1] Kampker A, Vallée D, Schnettler A. Elektromobilität. Berlin, Heidelberg: Springer; 2013.
[2] Keichel M, Schwedes O. Das Elektroauto: Mobilität im Umbruch. Wiesbaden: Springer Vieweg; 2013.
[3] Li S, Li K, Rajamani R, Wang J. Model predictive multi-objective vehicular adaptive cruise control. IEEE Transactions on Control Systems Technology; 2001; 19(3):556-566.
[4] Hellström E, Åslund J, Nielsen L. Design of an efficient algorithm for fuel-optimal look-ahead control. Control Engineering Practice 2010; 18(11):1318-1327.
[5] Sciaretta A, Guzella L. Control of hybrid electric vehicles. IEEE Control Systems Magazine 2007; 27(2):60-70.
[6] Boehme TJ, Schori M, Frank B, Schultalbers M, Lampe B. Solution of a hybrid optimal control problem for parallel hybrid vehicles subject to thermal constraints. 52nd IEEE Conference on Decision and Control; 2013; p. 2220-2226.
[7] Dib W, Serrao L, Sciaretta A. Optimal control to minimize trip time and energy consumption in electric vehicles. IEEE Vehicle Power and Propulsion Conference; 2011, p. 1-8.
[8] Petit N, Sciaretta A. Optimal drive of electric vehicles using an inversion-based trajectory generation approach. Preprints of the 18th IFAC World Congress; 2011, p. 14519-14525.
[9] Nocedal J, Wright SJ. Numerical Optimization 2nd ed. New York: Springer; 2006.
[10] Masjosthusmann C, Köhler U, Decius N, Büker U. A vehicle energy management system for a battery electric vehicle. IEEE Vehicle Power and Propulsion Conference (VPPC); 2012, p.339-344.
[11] Binder T, Blank L, Bock HG, Bulirsch R, Dahmen W, Diehl M, Kronseder T, Marquardt W, Schlöder JP, von Stryk O. Introduction to model based optimizatin of chemical processes on moving horizons. In: Grötschel M, Krumke SO, Rambau J, editors. Online Optimization of Large Scale Systems: State of the Art. Berlin: Springer; 2001. p. 295-340
[12] Hager WW. Rates of convergence for discrete approximations to unconstrained control problems. SIAM Journal on Numerical Analysis; 1976; 13(4):449-472.
[13] Dellnitz M, Schütze O, Hestermeyer T. Covering pareto sets by multilevel subdivision techniques. Journal of Optimization Theory and Applications 2005; 124:113-136.